J. Fluid Mech. (2006), *vol.* 564, *pp.* 395–414.
doi:10.1017/S0022112006001480 Printed in the United Kingdom

The settling velocity and shape distortion of drops in a uniform electric field

By XIUMEI XU AND G. M. HOMSY

Department of Mechanical and Environmental Engineering, University of California-Santa Barbara, Santa Barbara, CA 93106, USA

(Received 15 July 2005 and in revised form 3 March 2006)

We theoretically and experimentally investigate the settling velocity and deformation of a leaky dielectric liquid drop in a second leaky dielectric liquid subject to a uniform electric field, E. Both shape distortion and charge convection, when coupled with the asymmetric velocity profiles, will produce a net drag and a shift in the settling speed. Perturbation methods for small shape distortion and small charge convection are used to solve the problem. Corrections to the settling velocity from both contributions are combined linearly at the lowest order, and show a dependence on the drop size. The shape distortion due to charge convection is known to be asymmetric. Experiments are performed to measure the settling velocity and deformation of phenylmethylsiloxane-dimethylsiloxane (PMM) drops in castor oil. The experimental results are in qualitative agreement with the theory: the symmetric and asymmetric deformations and the change in settling velocity are all proportional to E^2, as predicted, and the settling speed shows the correct trends with drop size. Quantitative agreement is lacking, presumably due to the imprecision of the fluid properties, but the theory can fit all the data with reasonable choices for these properties.

1. Introduction

It is well known that liquid drops will be deformed when subjected to an external electric field. Taylor (1966) proposed an electrohydrodynamic theory based on a few assumptions: a neutrally buoyant drop, a quasi-static electric field, leaky dielectric fluids, weak deformation and no charge convection. There is no free bulk charge, but a small but finite conductivity coupled with a difference of dielectric constant and polarization allows charge to accumulate at the interface, so Taylor's theory is also called the 'leaky dielectric' model (Saville 1997). This accumulation of charge produces a non-zero tangential electric stress which drives a fluid motion and produces both tangential and normal hydrodynamic stresses. Shape deformation can be calculated as a perturbation from sphericity by balancing the normal electric and hydrodynamic stresses with the capillary pressure. Taylor's theory is in good qualitative agreement with the experimental results in predicting whether the deformation is prolate or oblate; however, Torza, Cox & Mason (1971) reported quantitative discrepancies between Taylor's theory and their extensive experimental measurements. Drops were found to be more deformed than the theoretical prediction for both prolate and oblate deformations. For prolate deformation, the deformation measurements are 2 to 4 times greater, and for the oblate case, 1 to 2 times greater than the theoretical predictions. Ajayi (1978) took into account higher-order terms in the shape distortion and predicted increased deformations for some of the fluid pairs of Torza *et al.*, but

this higher-order theory is insufficient to remove the discrepancy. Vizika & Saville (1992) carried out further experiments in which all the electrical properties of the liquids were measured. The drops were still found to be more deformed for prolate systems, but with better agreement with the theory, while the measurements for oblate systems were lower than the theoretical predictions. Feng (1999) computationally calculated deformation with the consideration of charge convection, and found that charge convection tends to enhance the prolate deformation and reduce the oblate deformation. These results help to explain Vizika & Saville's experimental measurements to some extent; however, Feng did not make a quantitative comparison because Vizika & Saville (1992) only provided the ratios of conductivity in their paper. In summary, although the basic phenomena are captured by the leaky dielectric model, there is still a lack of quantitative agreement between the theory and experiments; but as mentioned above, the theoretical calculations by Ajayi (1978) and Feng (1999) help to reduce the divergence to some extent. As we will see, this qualitative (but not quantitative) success of the theory will extend to our results as well.

For stationary drops with charge convection, the tangential electric stress is still antisymmetric with respect to the equatorial plane normal to the electric field. Therefore there is no drag for such neutrally buoyant drops, and the deformation remains symmetric. For translating drops, however, charge convection due to the asymmetric velocity breaks the antisymmetry of the electric stress and induces a net drag, and the deformation is no longer symmetric. Spertell & Saville (1976) took charge convection into account and theoretically calculated both shape distortion and the correction to the settling velocity of spherical drops in an electric field by perturbation theory for weak convection. We discuss their results in more detail below.

Settling velocity, shape distortion and charge convection are all coupled, i.e. one influences the other. Without charge convection, the electric and flow fields are coupled through the shape distortion. For drops undergoing translation, the asymmetric velocity and the shape distortion, acting together, produce a net drag and a shift in the settling speed. Therefore considering a settling drop in an electric field, by pursuing a perturbation analysis similar in spirit to that of Ajayi, we can calculate the correction to the settling velocity owing to shape distortion. On the other hand, when charge convection cannot be neglected, the electric and flow fields are additionally coupled through convection. There is also a shift in the settling speed even for spherical drops, and the deformation is altered by charge convection to be asymmetric: these two effects were the primary predictions of Spertell & Saville (1976).

The objective of this work is to study the coupling of settling velocity, shape distortion and charge convection theoretically and experimentally. Until now there is no experimental study of the settling velocity and deformation of a settling drop in an electric field. In fact, in order to avoid settling, previous experiments dealt with nearly isopicnic fluid pairs. Great efforts were made to mix fluids or find fluid pairs of similar densities; but there still exist some small density differences in many fluid pairs, as in Torza *et al.* (1971), where the typical density difference was $40\,\mathrm{kg\,m^{-3}}$. Therefore, they had to make the drop sizes small (seldom greater than 1 mm) to avoid settling, and this incurs a greater error in measurement. Since we expect settling drops to occur more commonly in applications, it is useful to extend the theory by the consideration of a mean settling velocity.

The problem is formulated with all assumptions and boundary conditions in § 2. In § 3, we present the solution procedure and results of the perturbation analysis for small shape distortion and recapitulate the calculation of Spertell & Saville (1976) for

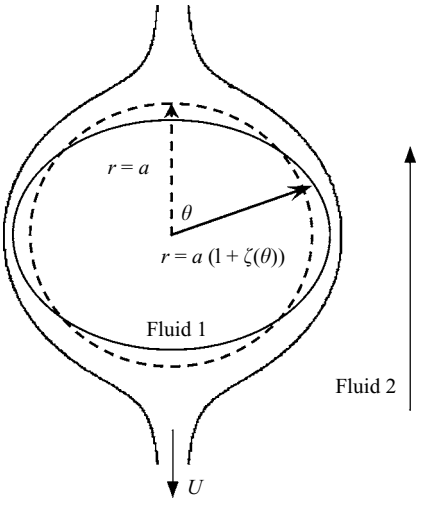

FIGURE 1. Schematic diagram of a translating drop in a uniform electric field.

weak charge convection, but in a more direct fashion than in their original exposition. In § 4, we discuss the experimental procedures and results of deformation and settling velocity measurement, and concluding remarks are made in § 5.

2. Problem formulation

We consider a leaky dielectric liquid drop suspended in a uniform flow of a second leaky dielectric fluid and subjected to a uniform external electric field as shown in figure 1. We denote the fluid viscosity, conductivity, dielectric constant and density by μ, σ, ε and ρ, and use a tilde to identify the drop phase. γ denotes the interfacial tension, U the velocity at infinity, E the electric field strength, and a the undeformed drop radius. $\boldsymbol{r}$, $\boldsymbol{\theta}$ are the radial and angular coordinates components in a spherical coordinate system whose origin is at the centre of the undeformed drop. The shape of the drop is taken to be axisymmetric, so there is no φ dependence. The deformed drop surface can be expressed as the dimensional radial position as a function of the azimuthal angle as $r = a(1 + \zeta(\theta))$, where $\zeta(\theta)$ is to be calculated as part of the solution.

2.1. *Scaling and dimensionless parameters*

We scale length by the radius of the undeformed drop a, and the surface charge by $\varepsilon\varepsilon_0 E$. There are two possible velocity scales: the electrohydrodynamic velocity and the settling velocity U. These two scales are driven by two independent and equally important mechanisms, the first of which is due to the applied external electric field E, while the second arises from the density difference between the drop and continuous phases. In like manner, there are two possible stress scales: an electric stress $\varepsilon\varepsilon_0 E^2$ and a viscous stress $\mu U/a$. In this analysis, we choose U as the velocity scale because it is more convenient when we calculate the correction to the settling velocity, and correspondingly we choose the viscous stress as the stress scale. In the electric part of the problem we use the electric field intensity at infinity E to scale the electric field, and in this way we keep $\varepsilon\varepsilon_0 E^2$ as the scale for the electric stress. The dimensionless parameter

$$W = \frac{a\varepsilon\varepsilon_0 E^2}{\mu U}, \tag{1}$$

gives the relative strength of these two stresses. Other important dimensionless numbers are:

$$Re=\frac{\rho U a}{\mu},\quad Ca=\frac{\mu U}{\gamma},\quad Re_E=\frac{\varepsilon\varepsilon_0 U}{a\sigma},\quad \lambda=\frac{\tilde{\rho}}{\rho},\quad R=\frac{\sigma}{\tilde{\sigma}},\quad M=\frac{\tilde{\mu}}{\mu},\quad Q=\frac{\tilde{\varepsilon}}{\varepsilon}. \tag{2}$$

The Reynolds number Re represents the relative strength of inertial force and viscous force, the capillary number Ca is the ratio of viscous forces to capillary forces, and the electric Reynolds number Re_E is the ratio of charge relaxation time $\varepsilon\varepsilon_0/\sigma$ to the flow time a/U. $Ca_E = CaW$ is the electric capillary number which gives the relative strength of the electric stress to that due to interfacial tension and curvature. Only two of the set of (Ca_E, Ca, W) are independent.

2.2. *Governing equations and boundary conditions*

We take the electric field to be quasi-static and determined in the usual way from a potential as $\boldsymbol{E}=-\nabla\Phi$. The electric potentials, outside and inside the drop, Φ, $\tilde{\Phi}$, satisfy Laplace's equation, the solutions of which can be expressed as:

$$\Phi=\sum_{n=0}^{\infty}\left(a_n r^n + b_n r^{-(n+1)}\right)P_n(\eta), \tag{3a}$$

$$\tilde{\Phi}=\sum_{n=0}^{\infty}\left(\tilde{a}_n r^n + \tilde{b}_n r^{-(n+1)}\right)P_n(\eta), \tag{3b}$$

in which $\eta=\cos\theta$, $P_n(\eta)$ is the nth order Legendre polynomial, and a_n, b_n and $\tilde{a}_n$, $\tilde{b}_n$ are unknown constants that must be determined.

Boundary conditions for the electric field are:

*e*1 the electric field is uniform at infinity;

*e*2 inside the drop the electric fields are bounded;

and at the interface:

*e*3 the tangential components of the electric field are continuous;

*e*4 charge convection balances charge conduction.

The first two boundary conditions *e*1 and *e*2 imply that some of the constants in (3) are zero: (4) gives the simplified expressions that satisfy these conditions.

$$\Phi=-r P_1(\eta)+\sum_{n=1}^{\infty} b_n r^{-(n+1)}P_n(\eta), \tag{4a}$$

$$\tilde{\Phi}=\sum_{n=1}^{\infty}\tilde{a}_n r^n P_n(\eta). \tag{4b}$$

Here b_n and $\tilde{a}_n$ are to be determined through the remaining boundary conditions.

In this study, the Reynolds number is assumed to be small, so inertial terms can be neglected in the momentum equation, and the flow is a Stokes flow. The associated streamfunctions Ψ,$\tilde{\Psi}$ satisfy:

$$E^4\Psi=0,\quad E^4\tilde{\Psi}=0. \tag{5}$$

The general solutions to (5) have the form of (Leal 1992):

$$\Psi=\sum_{n=1}^{\infty}(A_n r^{n+3}+B_n r^{n+1}+C_n r^{2-n}+D_n r^{-n})Q_n(\eta), \tag{6a}$$

$$\tilde{\Psi}=\sum_{n=1}^{\infty}(\tilde{A}_n r^{n+3}+\tilde{B}_n r^{n+1}+\tilde{C}_n r^{2-n}+\tilde{D}_n r^{-n})Q_n(\eta). \tag{6b}$$

Here, $Q_n(\eta)$ is the nth order Gegenbauer polynomial, and A_n, B_n, C_n D_n and $\tilde{A}_n$, $\tilde{B}_n$, $\tilde{C}_n$, $\tilde{D}_n$ are unknown constants that will be determined by applying boundary conditions.

Boundary conditions for the hydrodynamic problem are:

$f1$ uniform flow at infinity;

$f2$ inside of the drop the velocities are bounded;

and at the interface:

$f3$ the normal velocities are zero;

$f4$ the tangential velocities are continuous;

$f5$ the tangential viscous stresses are balanced with the electrical stresses;

$f6$ the jump in total normal stress is balanced by that due to interfacial tension.

By applying the first two boundary conditions $f1$ and $f2$, equation (6) can be simplified as:

$$\Psi = r^2 Q_1(\eta) + \sum_{n=1}^{\infty} (C_n r^{2-n} + D_n r^{-n}) Q_n(\eta), \tag{7a}$$

$$\tilde{\Psi} = \sum_{n=1}^{\infty} (\tilde{A}_n r^{n+3} + \tilde{B}_n r^{n+1}) Q_n(\eta), \tag{7b}$$

thus reducing the number of constants remaining to be determined through the remaining boundary conditions.

2.3. *Coupling between electric and flow fields*

In the following equations $\boldsymbol{T}$ represents the stress tensor, with subscripts t and n for tangential and normal components, subscripts H and E for the hydrodynamic and electric Maxwell stresses respectively, and $[\![\cdot]\!]$ denotes a jump across the drop surface, i.e. $[\![a]\!] = a - \tilde{a}$. All the variables and parameters are dimensionless. The Maxwell stresses are given by:

$$[\![(T_n)_E]\!] = \tfrac{1}{2}\left[\!\left[\kappa\left(E_n^2 - E_t^2\right)\right]\!\right], \tag{8a}$$

$$[\![(T_t)_E]\!] = [\![\kappa E_t E_n]\!], \tag{8b}$$

where $\kappa = 1$ on the medium phase side of the interface, and $\tilde{\kappa} = Q$ on the drop phase side. There are more complicated but standard expressions for the hydrodynamic stresses, which we do not write down.

The electric and flow fields are coupled through the three most important boundary conditions that hold at the interface, which in the dimensionless scaled coordinates is now at $r = 1 + \varsigma(\theta)$.

Tangential electric stress drives the fluid motion (boundary condition $f5$):

$$W[\![(T_t)_E]\!] + [\![(T_t)_H]\!] = 0. \tag{9}$$

The electric and hydrodynamic stress jumps involve the property ratios R and M in algebraically complicated but known ways.

The electric and flow fields determine the shape (boundary condition $f6$):

$$W[\![(T_n)_E]\!] + [\![(T_n)_H]\!] = Ca^{-1}\left(\rho_1^{-1} + \rho_2^{-1}\right), \tag{10}$$

where ρ_1 and ρ_2 are the two principal radii of curvature of the drop surface. Deformation is calculated by balancing the electric and viscous normal stress with interfacial tension, whereas shape distortion also affects the electric and flow fields.

Electric and flow fields are coupled through charge convection (boundary condition *e*4):

$$[\![\beta E_n]\!] = -Re_E \nabla_s \cdot (q V_s), \tag{11}$$

where $\beta = R$ on the medium phase side of the interface, and $\tilde{\beta} = 1$ on the drop phase side. $\nabla_s \cdot ( )$ is the surface divergence, and $\boldsymbol{V}_s$ the dimensionless surface velocity. The surface charge distribution in (11) is given by:

$$q = [\![\kappa E_n]\!]. \tag{12}$$

From (11), it is obvious that the importance of charge convection is measured by the electric Reynolds number Re_E. When Re_E is small, the right-hand side of (11) can be neglected, that is, the effect of charge convection can be neglected.

3. Solution procedure and results

The theoretical prediction of the shift in settling velocity is divided essentially into two parts. In the first part, we compute the shift due to shape deformation by small deformation theory. In the second part, we solve the problem for the shift due to charge convection for a spherical drop by perturbation in Re_E. Although this latter problem is identical to that solved by Spertell & Saville (1976), we obtain their results in a direct fashion. Finally, the two corrections are combined and the implications for experiments are discussed.

3.1. *Solution and results considering shape distortion only*

In this section, we assume there is no charge convection, and study the coupling of shape distortion and settling velocity. As we described in § 1, for drops undergoing translation, the asymmetric settling velocity coupled with shape distortion breaks the symmetry of the flow field and produces a net drag and a correction to the settling velocity. We employ an analysis similar to that of Taylor (1966) and Ajayi (1978) by assuming the electric capillary number Ca_E is small.

The drop surface can be expressed in general in a Legendre series:

$$r = 1 + \varsigma(\eta) = 1 + \sum_{n=0}^{\infty} \omega_n P_n(\eta), \tag{13}$$

where the ω_n determine the shape distortion. The ω_n are taken to be small and are related to the physical parameters of the problem through the interfacial boundary conditions. For small deformation, the curvature in (10) can be expressed as (Landau & Lifshitz 1959):

$$\rho_1^{-1} + \rho_2^{-1} = 2 - 2\varsigma - \frac{\mathrm{d}}{\mathrm{d}\eta}\left\{(1-\eta^2)\frac{\mathrm{d}\varsigma}{\mathrm{d}\eta}\right\}. \tag{14}$$

In the following expressions, the superscript represents the order of the perturbation. The zero-order (spherical drop) solution is a combination of Hadamard–Rybczynski and Taylor circulations.

$$\Psi^{(0)} = \left(r^2 - \frac{3M+2}{2(M+1)}r + \frac{M}{2(M+1)}r^{-1}\right)Q_1 + 2V_E(1-r^{-2})Q_2, \tag{15}$$

$$\tilde{\Psi}^{(0)} = \frac{1}{2(M+1)}(r^4 - r^2)Q_1 + 2V_E(r^5 - r^3)Q_2, \tag{16}$$

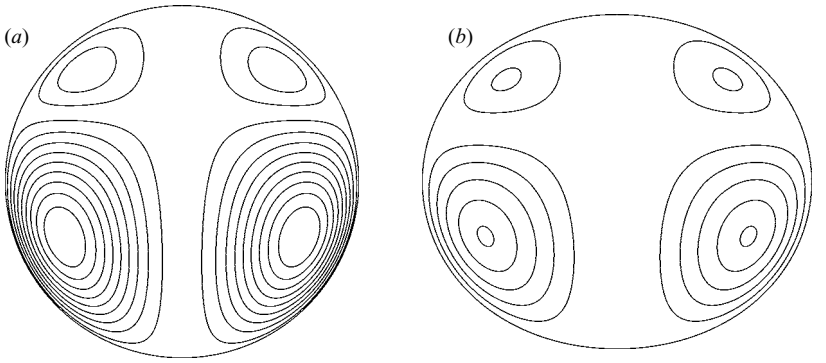

FIGURE 2. Schematic diagram of streamlines inside (*a*) a spherical drop; (*b*) a deformed drop.

where

$$V_E = -\frac{9R(1-RQ)}{10(M+1)(2R+1)^2}W \tag{17}$$

is the dimensionless maximum velocity at the interface and appears as a key parameter in other analyses of drops in electric fields (Chang, Carleson & Berg 1981; Ward & Homsy 2001, 2003).

The first-order shape distortion is determined by the zero-order electrical and viscous normal stresses. Substituting the zero-order solutions into the boundary condition of normal stress balance (equation (10)), we find the only Legendre polynomial required in (13) is P_2, and the first-order shape distortion is that calculated by Taylor (1966):

$$\omega_2^{(1)} = \frac{9Ca_E}{4(2R+1)^2}\left[\tfrac{1}{3}(1+R^2-2QR^2) + \frac{R(1-QR)(2+3M)}{5(M+1)}\right]. \tag{18}$$

From the analysis of Taylor & Acrivos (1964), a uniform flow will not alter the shape of the drop in a Stokes flow, so the deformation is caused entirely by the electric stress.

Figure 2 gives the schematic diagram of the streamlines inside a spherical and deformed drop. At zero order (spherical drop), for given fluid properties and W (equivalently V_E), the flow is given by (15) and (16). The shape distortion will affect the electric field and hence the electric stress. Since the electric field is still quasi-static and there is no charge convection, the problem for $\Phi^{(1)}$, $\tilde{\Phi}^{(1)}$ still reduces to Laplace's equation, subject to $[\![E_t]\!] = 0$, $[\![\beta E_n]\!] = 0$ on the distorted shape. After these first-order fields are found, the perturbations to the electric stress are used to solve the flow problem subject to (9) and $f3$ and $f4$ on the distorted shape. Thus we use the first-order deformation to correct the electric and flow fields. At the deformed drop surface $r = 1 + \omega_2^{(1)} P_2$, the normal and tangential unit vectors $\boldsymbol{n}$, $\boldsymbol{t}$ are different from the spherical coordinates $\boldsymbol{r}$ and $\boldsymbol{\theta}$. Let α denote the angle between $\boldsymbol{n}$ and $\boldsymbol{r}$. Assume the electric capillary number is small, i.e. $|\omega_2^{(1)}| \ll 1$, therefore,

$$\alpha \cong \tan(\alpha) = \omega_2^{(1)} \frac{\mathrm{d}P_2}{\mathrm{d}\theta}. \tag{19}$$

Then we can express the normal and tangential components of any vector at the deformed drop surface in terms of their spherical components as:

$$A_n[r] = A_r[r] - \omega_2^{(1)} \frac{\mathrm{d}P_2}{\mathrm{d}\theta} A_\theta[r], \tag{20}$$

$$A_t[r] = A_\theta[r] + \omega_2^{(1)} \frac{\mathrm{d}P_2}{\mathrm{d}\theta} A_r[r]. \tag{21}$$

The bracket notation is as follows. $A_n[r]$ (for example) denotes a quantity evaluated on the actual (deformed) surface, $r = 1 + \varsigma(\theta)$, while $A_n[1]$ indicates the quantity evaluated at the undeformed surface $r = 1$. Assuming A_r and A_θ can be expressed as perturbation expansions in powers of $\omega_2^{(1)}$, we can expand (20) to the first order as:

$$A_n[r] = A_r^{(0)}[r] + \omega_2^{(1)} A_r^{(1)}[r] - \omega_2^{(1)} \frac{\mathrm{d}P_2}{\mathrm{d}\theta} \left(A_\theta^{(0)}[r] + \omega_2^{(1)} A_\theta^{(1)}[r] \right). \tag{22}$$

In (22), $\omega_2^{(1)}$ appears both explicitly as the perturbation parameter and implicitly in the argument of the drop surface r. By doing a Taylor series expansion about the spherical drop surface at $r = 1$ in the usual way, and keeping only the linear terms in $\omega_2^{(1)}$, we can rewrite (22) as:

$$A_n[r] = A_r^{(0)}[1] + \omega_2^{(1)} \left(A_r^{(1)}[1] + P_2 \frac{\partial A_r^{(0)}}{\partial r}[1] - A_\theta^{(0)}[1] \frac{\mathrm{d}P_2}{\mathrm{d}\theta} \right), \tag{23}$$

and in the same way, (21) can be expanded as:

$$A_t[r] = A_\theta^{(0)}[1] + \omega_2^{(1)} \left(A_\theta^{(1)}[1] + P_2 \frac{\partial A_\theta^{(0)}}{\partial r}[1] + A_r^{(0)}[1] \frac{\mathrm{d}P_2}{\mathrm{d}\theta} \right). \tag{24}$$

With (23) and (24), we are able to transform the boundary conditions at the deformed drop surface to those on the spherical surface.

Equations (23, 24) make it clear that $\omega_2^{(1)}$ is the small perturbation parameter, and from (18), it is proportional to the electric capillary number Ca_E. Therefore, we express the electric potential and the streamfunction up to the first order as: $\varphi = \varphi^{(0)} + \omega_2^{(1)} \varphi^{(1)}$, $\psi = \psi^{(0)} + \omega_2^{(1)} \psi^{(1)}$. A tedious but straightforward calculation gives the non-zero constants in the electric potentials (equation (3)) as:

$$b_1^{(1)} = \frac{6}{5} \frac{(R-1)^2}{(2R+1)^2}, \quad b_3^{(1)} = -\frac{9}{5} \frac{R-1}{2R+1}, \quad \tilde{a}_1^{(1)} = \frac{18}{5} \frac{R(R-1)}{(2R+1)^2}, \tag{25}$$

and the non-zero constants in the streamfunctions (equation (6)) as:

$$\left.\begin{aligned} &C_1^{(1)} = \frac{3M^2 - M + 8}{10(M+1)^2}, \quad D_1^{(1)} = -\frac{3(M^2 - M + 2)}{10(M+1)^2}, \quad C_2^{(1)} = \left(\frac{24(1-R)}{5(2R+1)} + \frac{12(1-M)}{35(M+1)} \right) V_E, \\ &D_2^{(1)} = \left(-\frac{24(1-R)}{5(2R+1)} - \frac{8(4+M)}{35(M+1)} \right) V_E, \quad C_3^{(1)} = -\frac{63M + 54}{35(M+1)}, \quad D_3^{(1)} = \frac{63M + 12}{35(M+1)}, \\ &C_4^{(1)} = \frac{92}{21} V_E, \quad D_4^{(1)} = -\frac{164}{21} V_E; \end{aligned}\right\} \tag{26}$$

and

$$\left.\begin{aligned}
&\tilde{A}_1^{(1)} = \frac{4-2M}{5(M+1)^2}, \quad \tilde{B}_1^{(1)} = \frac{3(M-1)}{5(M+1)^2}, \quad \tilde{A}_2^{(1)} = \left(\frac{24(1-R)}{5(2R+1)} - \frac{62M+38}{35(M+1)}\right)V_E \\
&\tilde{B}_2^{(1)} = \left(-\frac{24(1-R)}{5(2R+1)} + \frac{42M+18}{35(M+1)}\right)V_E, \quad \tilde{A}_3^{(1)} = \frac{6}{7(M+1)}, \quad \tilde{B}_3^{(1)} = -\frac{72}{35(M+1)} \\
&\tilde{A}_4^{(1)} = \frac{8}{3}V_E, \quad \tilde{B}_4^{(1)} = -\frac{128}{21}V_E.
\end{aligned}\right\} \tag{27}$$

As is well known (Leal 1992), the drag on an axisymmetric body is related to the expansion of the streamfunction (equation (6)) by:

$$\begin{aligned}
F_D &= 4\pi\mu U a C_1, \\
&= 4\pi\mu U a\left(-\frac{3M+2}{2(M+1)} + \varpi_2^{(1)}\frac{3M^2-M+8}{10(M+1)^2}\right), \\
&= 4\pi\mu U a\left(-\frac{3M+2}{2(M+1)} + \frac{9(3M^2-M+8)}{40(M+1)^2(2R+1)^2}\left[\tfrac{1}{3}(1+R^2-2QR^2)\right.\right. \\
&\quad \left.\left. + \frac{R(1-QR)(2+3M)}{5(M+1)}\right]Ca_E\right).
\end{aligned} \tag{28}$$

The leading term in (28) is, of course, the Stokes drag on a spherical droplet, and is the key result. Anticipating our experiments on settling drops, we balance the drag with the net buoyant force and calculate the settling velocity. Equation (29*a*) gives the resulting expression for the settling velocity normalized by the Hadamard–Rybczynski velocity U_H. Since in the perturbation method, the electric capillary number is assumed to be small, (29*b*) is the binomial expansion of (29*a*) to the first order.

$$\frac{U}{U_H} = \frac{1}{1 - \dfrac{9(3M^2-M+8)}{20(2R+1)^2(M+1)(3M+2)}\left[\tfrac{1}{3}(1+R^2-2QR^2) + \dfrac{R(1-QR)(2+3M)}{5(M+1)}\right]Ca_E}, \tag{29a}$$

$$= 1 + \frac{9(3M^2-M+8)}{20(2R+1)^2(M+1)(3M+2)}\left[\tfrac{1}{3}(1+R^2-2QR^2) + \frac{R(1-QR)(2+3M)}{5(M+1)}\right]Ca_E + O(Ca_E^2), \tag{29b}$$

where

$$U_H = \frac{2}{9}\frac{ga^2(\tilde{\rho}-\rho)}{\mu}\frac{M+1}{M+\frac{2}{3}}. \tag{30}$$

Equation (29) is the main result in this section, which gives the correction to the settling velocity for small distortions. Notice that in (29*b*), $(3M^2 - M + 8) > 0$, so the sign of the correction is determined by the term in square brackets, which is known as Taylor's discriminant. When Taylor's discriminant is positive, the shape of the drop is prolate and the drop falls faster; when negative, the shape is oblate and the drop falls slower. This is reasonable since the correction to the drag is entirely due to shape distortion. When distortion results in oblate shapes, the drag increases because of the increase of cross-sectional area in the flow direction, and vice versa for prolate distortion.

3.2. *Solution and results considering charge convection only*

Spertell & Saville (1976) calculated the correction to the settling velocity and the deformation due to weak charge convection. Although their results are correct, their

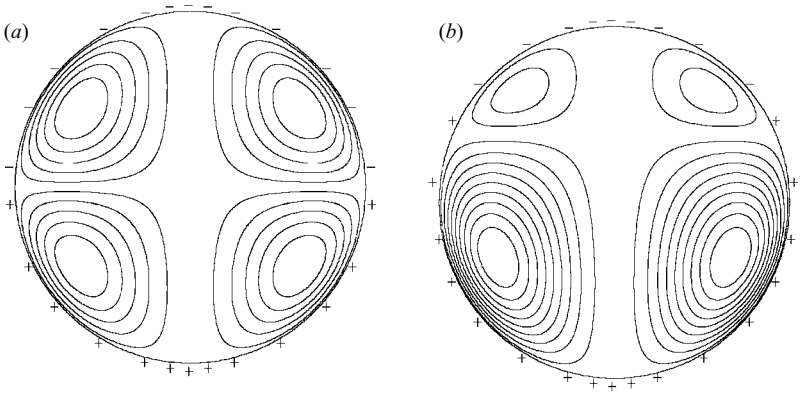

FIGURE 3. Schematic diagram of streamlines and charge distribution in (*a*) a neutrally buoyant spherical drop; (*b*) a settling spherical drop.

analysis is complicated. They use γ/a to scale stress, and let both Ca and Ca_E be small parameters in their perturbation method. Recognizing that the proper perturbation parameter is implied by (11), i.e. the electric Reynolds number Re_E, we can simplify Spertell & Saville's calculation.

Figure 3 shows a schematic diagram of the streamlines and charge distribution with charge convection for a neutrally buoyant and settling spherical drop, respectively. Without settling, the charge distribution, while influenced by convection, is still antisymmetric with respect to the equatorial plane. So the corrected flow field is antisymmetric and there is no drag. With settling, however, the asymmetric settling speed coupled with charge convection results in a charge distribution that is no longer antisymmetric about the equatorial plane; as a result, there is a net drag and a corresponding change in settling speed.

Since the domain is spherical to leading order, the solution procedure is straightforward. First, we evaluate the convective term $\nabla_s \cdot (q V_s)$ from the zero-order solutions and calculate the disturbed electric field. Then, the flow field is solved by applying boundary conditions (9), $f3$ and $f4$ on a sphere, and the shape distortion can be corrected by computing the total normal stress. For a spherical drop, charge convection corrects the zero-order solution as $\psi = \psi^{(0)} + Re_E \psi^{(1)} + O(Re_E^2)$. (Note that although we use the same notation, the first-order streamfunction $\psi^{(1)}$ we solve for is different from the one in § 3.1.)

The electric and flow fields are now coupled through the effect of charge convection, so the first-order electric field is corrected by the zero-order solutions by expanding (11) in spherical coordinates:

$$\left[\!\left[\beta E_n^{(1)}\right]\!\right] = -Re_E \frac{1}{r \sin\theta} \frac{\partial\left(\left[\!\left[\kappa E_n^{(0)}\right]\!\right] v_\theta^{(0)} \sin\theta\right)}{\partial\theta}. \tag{31}$$

We obtain the non-zero constants in (3) as:

$$\left.\begin{aligned} &\tilde{a}_n^{(1)} = b_n^{(1)} \\ &b_1^{(1)} = -\frac{12R(1-RQ)}{5(2R+1)^2} V_E, \quad b_2^{(1)} = -\frac{3R(1-RQ)}{(2R+1)(3R+2)(M+1)}, \\ &b_3^{(1)} = -\frac{48R(1-RQ)}{5(2R+1)(4R+3)} V_E. \end{aligned}\right\} \tag{32}$$

By applying boundary conditions (9), $f3$ and $f4$ on a sphere, we obtain the first-order flow field as:

$$C_n^{(1)} = \tilde{A}_n^{(1)} = -D_n^{(1)} = -\tilde{B}_n^{(1)}, \tag{33a}$$

$$C_1^{(1)} = \frac{2(3R - RQ + 3)}{3(3R + 2)(M + 1)} V_E, \tag{33b}$$

$$C_2^{(1)} = \frac{8}{5}\left[\frac{12(4R - RQ + 4)}{7(4R + 3)} - \frac{2R + 2RQ - 1}{2R + 1}\right] V_E^2, \tag{33c}$$

$$C_3^{(1)} = -\frac{12(3R + 4RQ - 2)}{7(3R + 2)(M + 1)} V_E, \tag{33d}$$

$$C_4^{(1)} = -\frac{320(4R + 6RQ - 3)}{63(4R + 3)} V_E^2. \tag{33e}$$

Since C_1 is known, the correction to the settling velocity can be calculated as before,

$$\frac{U}{U_H} = \frac{1}{1 + \dfrac{6R(1 - RQ)(3R - RQ + 3)}{5(2R + 1)^2(3R + 2)(3M + 2)(M + 1)} WRe_E}, \tag{34a}$$

or since Re_E is assumed small,

$$\frac{U}{U_H} = 1 - \frac{6R(1 - RQ)(3R - RQ + 3)}{5(2R + 1)^2(3R + 2)(3M + 2)(M + 1)} WRe_E + O\left(Re_E^2\right). \tag{34b}$$

Considering charge convection also makes further corrections to the first-order Taylor deformation (equation (18)), which as is well-known, is proportional to aE^2.

Substituting the first-order solutions (equations (32) and (33)) into (10), we calculate the higher-order non-zero terms in (13) as:

$$\omega_2^{(2)} = \left(\frac{24(2M + 3)(4R - RQ + 4)}{35(4R + 3)} + \frac{16MR + 4R + 76MRQ + 64RQ + 22M + 28}{15(2R + 1)}\right) \times Re_E V_E^2 Ca, \tag{35a}$$

$$\omega_3^{(2)} = \frac{132MRQ - 6MR + 120RQ + 39M - 15R + 45}{35(3R + 2)(M + 1)} Re_E V_E Ca, \tag{35b}$$

$$\omega_4^{(2)} = \frac{8(102MRQ - 16RM + 33M - 20R + 96RQ + 36)}{189(4R + 3)} Re_E V_E^2 Ca. \tag{35c}$$

As mentioned, (34) and (35) are originally due to Spertell & Saville (1976). The effect of charge convection coupled with the settling velocity causes the shape distortion to be asymmetric. (Similar asymmetric shapes have been calculated for conducting drops with a net surface charge in a field by Adornato & Brown (1983), who also used perturbation methods for weak distortion. The origins of the asymmetry are very different in the two problems, however. In Adornato & Brown, it is due to a third-order coupling between a point source and a dipole, while in Spertell & Saville (1976), it appears at second order for the reasons stated above.) In (35), $\omega_3^{(2)}$ is antisymmetric with respect to the equatorial plane, while others are symmetric, so the net shape distortion is asymmetric. Analysing the magnitude of the terms in (35) in orders of the electric field strength, we find both $\omega_2^{(2)}$ and $\omega_4^{(2)}$ are proportional to aE^4, while $\omega_3^{(2)}$is proportional to E^2, independent of a.

Following other investigators, we define the deformation D as the difference of the lengths of the axes parallel and perpendicular to the electric field divided by their

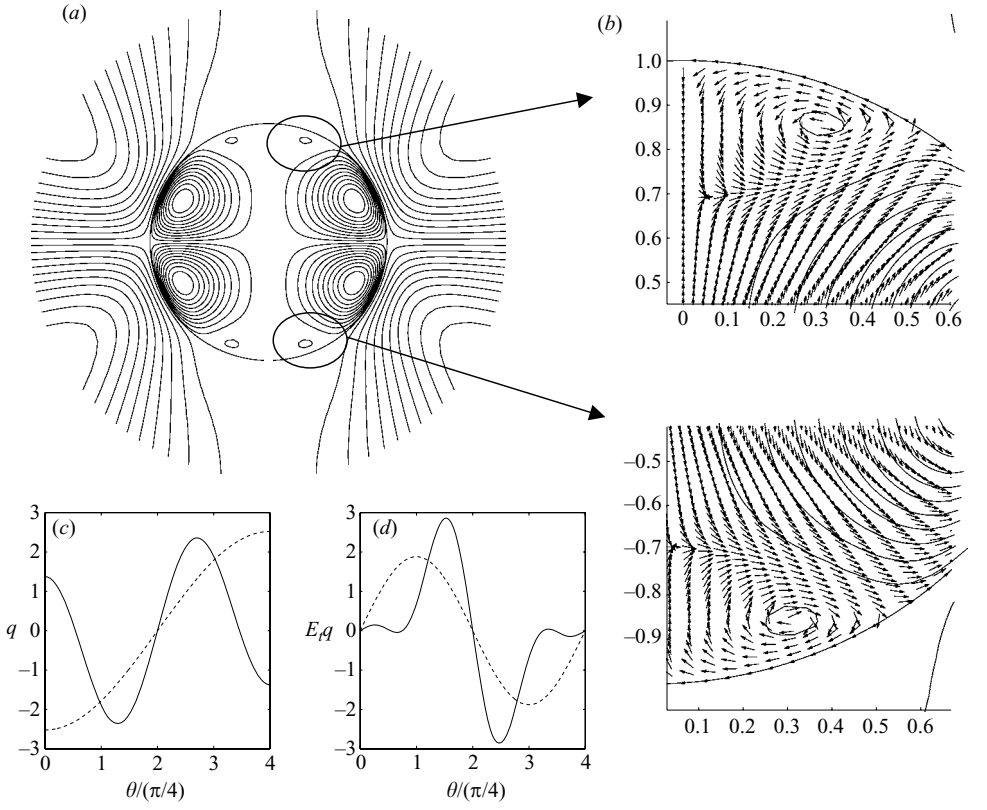

FIGURE 4. Effect of charge convection without settling: $R = 100$, $Q = 1.7$, $M = 0.03$, $W = 2.7$, $Ca = 0.1$, $Re_E = 0.18$, (*a*) streamlines, (*b*) magnified normalized velocity vectors, (*c*) charge distribution, (*d*) tangential electric force. In (*c*) and (*d*) dashed lines are the zero-order solutions.

sum: $D > 0$ or $D < 0$ for prolate and oblate deformations, respectively. From the above, we have the full expression of the deformation as:

$$D = \frac{3\omega_2^{(1)} + \left(3\omega_2^{(2)} + \frac{5}{4}\omega_4^{(2)}\right)}{4 + \omega_2^{(1)} + \omega_2^{(2)} + \frac{11}{4}\omega_4^{(2)}}. \tag{36}$$

The term in brackets is due to the contribution of charge convection, and it is always positive. This is consistent with Feng's numerical results that charge convection always enhances prolate deformation and reduces oblate deformation.

The antisymmetric shape distortion $\omega_3^{(2)}$ cancels in the expression of D: therefore, this measure of deformation is incomplete for asymmetric distortions. In order to measure the antisymmetric distortion we define AD as the difference of the radii parallel to the electric field divided by their sum. Equation (37) gives the expression:

$$AD = \frac{r_2 - r_1}{r_2 + r_1} = \frac{\omega_3^{(2)}}{1 + \omega_2^{(1)} + \omega_2^{(2)} + \omega_4^{(2)}}, \tag{37}$$

and since $\omega_3^{(2)}$is proportional to E^2, AD has the same E^2 dependence.

To help explain the coupling of charge convection and settling, the flow fields are plotted for neutrally buoyant and settling drops, respectively. Figure 4 shows

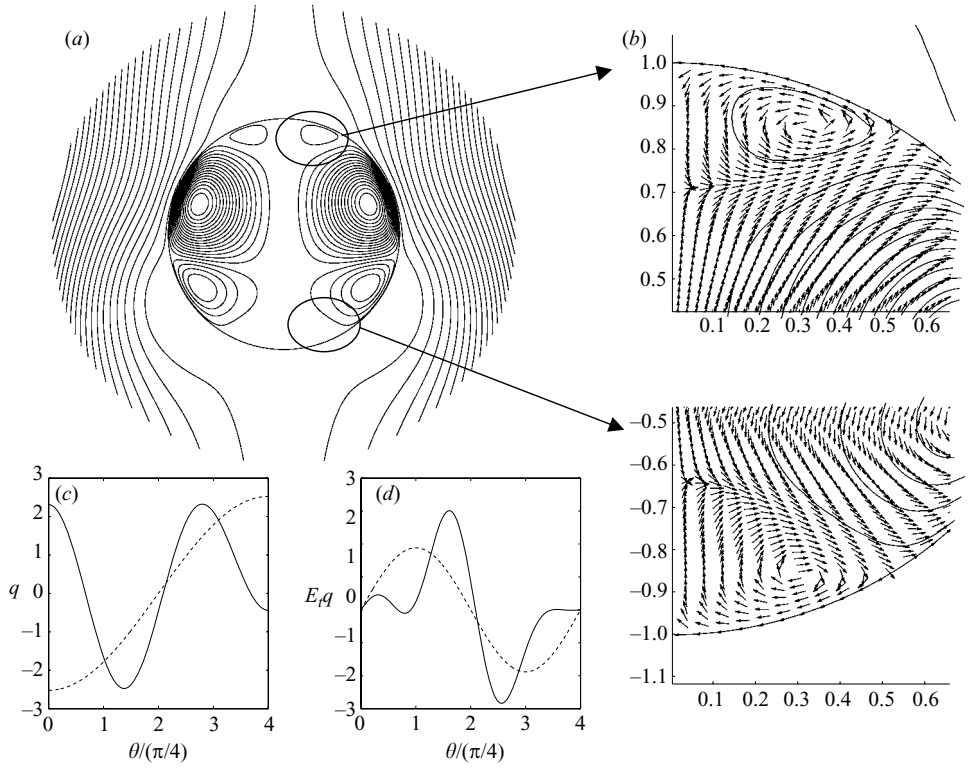

FIGURE 5. Effect of charge convection with settling: $R = 100$, $Q = 1.7$, $M = 0.03$, $W = 2.7$, $Ca = 0.1$, $Re_E = 0.18$, (*a*) streamlines, (*b*) magnified normalized velocity vectors, (*c*) charge distribution, (*d*) tangential electric force. In (*c*) and (*d*) dashed lines are the zero-order solutions.

the theoretical results of the effects of charge convection for a suspended spherical drop, with the choice of physical properties as $R = 100$, $Q = 1.7$, $M = 0.03$, $W = 2.7$, $Ca = 0.1$, $Re_E = 0.18$. (For neutrally buoyant drops, the velocity scale is given by the electro-hydrodynamic velocity V_E, so the dimensionless number W is calculated from (17).) Figure 4(*c*) shows the charge density distribution plotted *vs.* the azimuthal angle θ. We see that although charge convection significantly alters the charge distribution, it does not break the antisymmetry about the equatorial plane. As expected, the flow field remains antisymmetric, and there is no net drag. The influence of charge convection on the flow field can be easily observed from the plot of streamlines (figure 4*a*) and the normalized velocity field (figure 4*b*): near the poles there are small induced vortices. The plot of tangential electric force (figure 4*d*) shows sign reversals of the electric force, which drive these small vortices. The magnitudes of the induced vortices are small compared to the main vortices, which is obvious in figure 4(*a*, *d*).

Figure 5 gives corresponding results for a settling spherical drop with the same physical properties as in figure 4. Figures 5(*c*) and 5(*d*) clearly show that the settling coupled with charge convection breaks the antisymmetry of the charge distribution and electric force about the equatorial plane, and hence the flow field is as shown in figure 5(*a*). There are small vortices induced near the poles in a similar way to before, but owing to the asymmetry of the stresses, the magnitudes of the induced vortices at the top and bottom poles are different.

3.3. *Combining the two effects*

We have calculated the corrections to the settling velocity due to shape distortion and charge convection in two separate perturbation methods, which, at the lowest order, can be combined linearly. In (29) and (34) we express the corrections in dimensionless parameters. However, when performing experiments for fixed fluid pairs with all properties fixed, we usually vary drop size a and electric field strength E. Therefore, we write the results in dimensional form as:

$$U_s = 1 + X_1 a E^2 + X_2 E^2 + \text{h.o.t}, \tag{38}$$

where

$$X_1 = \frac{\varepsilon\varepsilon_0}{\gamma} \frac{9(3M^2 - M + 8)}{20(2R+1)^2(M+1)(3M+2)} \left[\tfrac{1}{3}(1 + R^2 - 2QR^2) + \frac{R(1-QR)(2+3M)}{5(M+1)}\right], \tag{39}$$

$$X_2 = -\frac{(\varepsilon\varepsilon_0)^2}{\mu\sigma} \frac{6R(1-RQ)(3R-RQ+3)}{5(2R+1)^2(3R+2)(3M+2)(M+1)}, \tag{40}$$

are dimensional quantities that depend only on fluid properties.

In (38), both terms are proportional to E^2 because both corrections are driven by the electric Maxwell stress which has the E^2 dependence from (8). The term involving X_1 is due to the shape distortion, so it is also proportional to the drop radius a, whereas that involving X_2 does not depend on a because it is due to the effect of charge convection. For most fluid pairs in the experimental work of Torza *et al.* (1971) and Vizika & Saville (1992), the coefficients X_1 and X_2 have opposite signs, which indicates the existence of critical drop size determining whether the settling velocity is greater or less than U_H. This critical size is given by:

$$a_c = \frac{40R(1-RQ)(3R-RQ+3)(M+1)}{(3R+2)(3M^2-M+8)[5(M+1)(1+R^2-2R^2Q)+3(3M+2)(R-R^2Q)]} \frac{\varepsilon\gamma}{\mu\sigma}. \tag{41}$$

By substituting in the fluid parameters given by Torza *et al.* (1971), we find the typical value of the critical drop size is small, in the range of 10^{-9} – 10^{-3} m.

As described in § 3.1, X_1 always has the same sign as $\omega_2^{(1)}$. So if Taylor's deformation is dominant in the expression for the deformation (equation (36)), then although charge convection will make a correction, we are still able to tell the sign of X_1 from whether the distortion is prolate or oblate.

4. Experiments

We carried out experiments to measure the deformation and settling velocity of liquid drops. In this section the experimental set-up and procedure are described, followed by results.

4.1. *Apparatus*

The experiments are performed in a 12 cm high acrylic cell equipped with two copper electrodes $12 \times 12\,\text{cm}^2$ and 0.3 cm thick on the top and bottom. The drops were injected using 100 and 200 µl pipettes. In order to guarantee the drop sizes are identical in a series of experiments, only one drop is inserted at the beginning, and when the drop falls near the bottom, the tank is tipped over to begin the next experiment. An electric field is applied across the electrodes from a Spellman high-voltage power supply (output range from 0 to 30 KV). The voltage is increased systematically in a series of

Fluid	Density ($\mathrm{kg\,m^{-3}}$)	Dielectric constant	Conductivity ($\mathrm{S\,m^{-1}}$)	Viscosity ($\mathrm{kg\,ms^{-1}}$)
PMM	1000	2.8	$(0.25 \sim 1)10^{-12}$	0.5
Castor oil	957–961	4.45	$10^{-9} \sim 10^{-11*}$	1.4

* The conductivity of castor oil is $10^{-9}\,\mathrm{S\,m^{-1}}$, as given by Torza *et al.* (1971). Vizika & Saville (1992) give the conductivity ratio of silicone oil to castor oil as approximately 10^{-2}. Gelest gives the conductivity of silicone oil as $10^{-13}\,\mathrm{S\,m^{-1}}$. From Vizika & Saville's ratio, we obtain another possible conductivity of castor oil as $10^{-11}\,\mathrm{S\,m^{-1}}$.

TABLE 1. Physical properties of the fluids.

experiments, and at the end, measurements are repeated at zero electric field to verify the purity of the drop and lack of any surface contamination. Movies of the experiments were recorded using a Canon XL1 CCD camera fitted with a Sigma MACRO 105 mm F2.8 EX lens, and drop sizes are determined from the calibrated still images.

We use castor oil from Fisher® as the medium phase and phenylmethylsiloxane-dimethylsiloxane (PMM) from Gelest as the drop phase. All the physical parameters of PMM are obtained from Gelest, and the parameters of castor oil are estimated from the data given by Fisher® and other investigators. Castor oil easily absorbs water, so its dielectric constant can vary significantly (D. A. Saville, personal communication 2005), and there is no agreed-upon value of its conductivity. Table 1 gives estimates of all the physical parameters.

We chose this fluid pair mainly because the density difference is large ($40\,\mathrm{kg\,m^{-3}}$), so the settling velocity is large enough to overcome small errors in measurement. Because the fluids are very viscous and the drop size is small (two drop sizes are used, 2.8 mm and 3.3 mm), the Reynolds number is of the order of 10^{-3}. Therefore, the Stokes flow assumption is satisfied. We only let the drop move in the middle of the tank to minimize wall effects. We estimate the error due to sidewalls to be about 8 % (from the results of Keh & Chen 2001), and from the error due to the bottom wall to be about 5 % (from the results of Wacholder & Weihs 1972).

4.2. *Experimental procedure*

The CCD camera is focused on the middle 2 cm of the tank. After a drop is inserted, the power supply is turned on. When the drop falls into view, the digital camcorder is started in order to record the falling process. The voltage is increased systematically in a series of experiments. The video images are saved in bitmap format, which is a discretized matrix representation of the actual image. The deformation can be determined as:

$$D = \frac{l_1 - l_2}{l_1 + l_2}, \tag{42}$$

where l_1 and l_2 are the lengths of drop axes parallel and perpendicular to the applied electrical field, respectively. The settling velocity is determined by

$$U_s = \frac{mp}{t}. \tag{43}$$

Here m is the number of pixels that the drop's top boundary moves in two frames, p the pixel size ($\sim 50\,\mu\mathrm{m}$), and t the time difference between the two frames. To measure the symmetric deformation, we need only the lengths of drop axes; the measurement of the

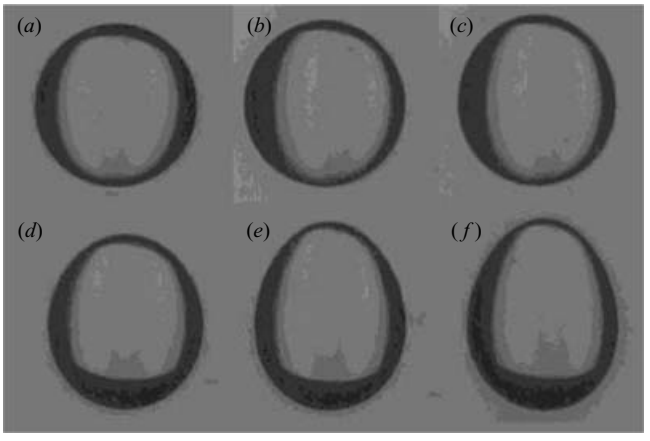

FIGURE 6. Shape distortion of a 3.3 mm PMM drop in castor oil. (*a*) $E = 0\,\mathrm{KV\,m^{-1}}$, (*b*) $E = 41.6\,\mathrm{KV\,m^{-1}}$, (*c*) $E = 66.7\,\mathrm{KV\,m^{-1}}$, (*d*) $E = 91.7\,\mathrm{KV\,m^{-1}}$, (*e*) $E = 125\,\mathrm{KV\,m^{-1}}$, (*f*) $E = 150\,\mathrm{KV\,m^{-1}}$.

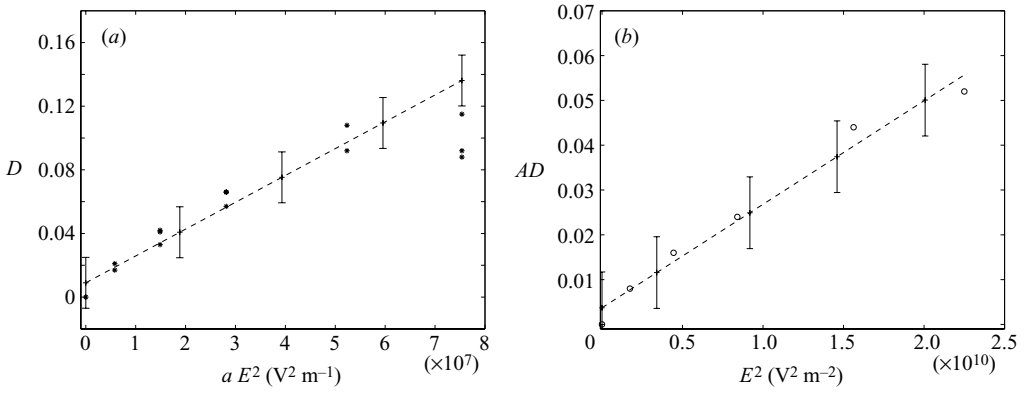

FIGURE 7. For the 3.3 mm drop, (*a*) deformation plotted *vs.* aE^2; (*b*) the asymmetric deformation plotted *vs.* E^2. The dashed lines are linear fits to the data, and error bars give the pixel error.

asymmetric deformation is more complicated because it relies on an accurate determination of the centre of the equivalent undistorted spherical drop. We discretize the bitmap image horizontally to obtain the boundary of the drop as a function of the axial position. By smoothing these discretized data into a continuous curve, we can diminish the influence of pixel noise. The position of the drop axis parallel to the electric field can be determined as the mean of the left and right boundaries, since the drop remains axisymmetric. With the position of the axis and the smooth boundary, we calculate the centre of mass by simple quadratures, giving the coordinate of the centre of the equivalent spherical drop. The asymmetric deformation is then computed simply from (37).

4.3. *Experimental results and comparison with theory*

Deformation

Figure 6 shows images of a 3.3 mm drop under several electric field strengths, and figure 7 plots the deformation measurements for the same drop. In figure 7(*a*),

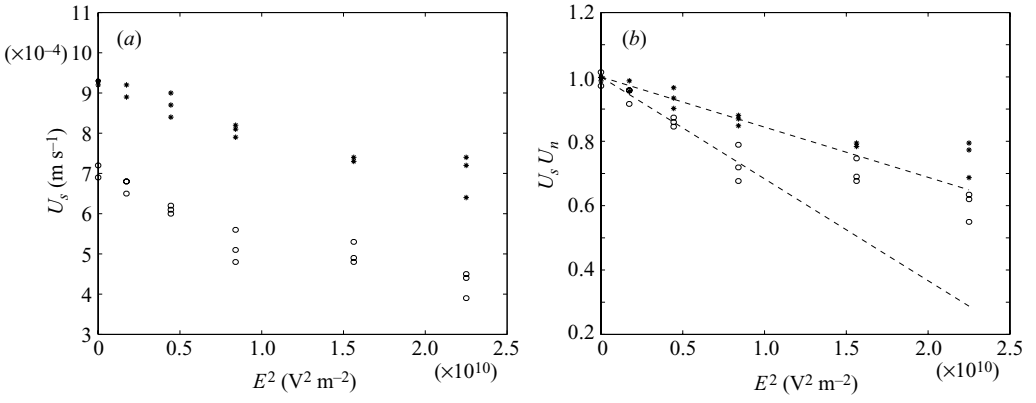

FIGURE 8. Settling velocity measurement for 2.8 'o' and 3.3 '*' mm drops plotted *vs.* E^2, (*a*) dimensional settling velocity measurements, (*b*) same velocity measurements but normalized with the Hadamard–Rybczynski velocity. The dashed lines are linear fits to the data at low fields.

each '*' represents one experimental measurement, and the error bars give the pixel error. At low fields, the deformation is linear in aE^2, as expected. The dashed line is a linear interpolation of data except for those at the highest electric field which obviously deviate from linearity and the interpolating slope is $1.91 \times 10^{-9}\,\mathrm{m\,V^{-2}}$. Figure 7(*b*) plots the asymmetric deformation *vs.* E^2, in which the '○' represent the average measurements. As expected, the asymmetric deformation is proportional to E^2. The dashed line is a linear interpolation of the average measurements, and the interpolating slope is $2.3 \times 10^{-12}\,\mathrm{V^{-2}}$.

Settling velocity

Figure 8(*a*) shows settling velocity measurements for the 2.8 mm and 3.3 mm drops represented by '○' and '*', respectively. There is scatter in the data, but it is apparent that the settling velocity decreases with an increase of electric field strength. For both drop sizes, the slopes diminish at high fields, which may be due to a combination of the higher-order terms in the binomial expansions of (29*b*) and (34*b*), and the higher-order effects that the leading-order perturbation theory cannot capture.

We linearly interpolate the data at low fields and get the Hadamard–Rybczynski velocity U_H from the intersection at $E = 0$. The ratio of these velocities (1.31) compares well with the square of the radius ratio (1.39). We rescale the settling velocity measurements by U_H as in figure 8(*b*), the dashed lines being a linear interpolation of the data at lower fields.

Comparison with theory

The deformation is always prolate: from the discussion in § 3, $X_1 > 0$, and for most fluid pairs, $X_1 \cdot X_2 < 0$, so we infer that $X_2 < 0$. From figure 8(*a*), the settling velocity decreases with the increasing electric field, so the X_2 term, i.e. the charge convection term, is dominant in the corrections (equation (38)). This indicates that an increase in drop size will decrease the slope, which is seen in figure 8(*b*). As already mentioned, the measurements of deformation D and asymmetric deformation AD are proportional to E^2 as expected. Therefore, all the experimental results are in qualitative agreement with the theory; but the deformation calculated for small charge convection alone cannot explain why the deformation at the highest field is less deformed than linearity predicts, since the theory predicts that the higher-order

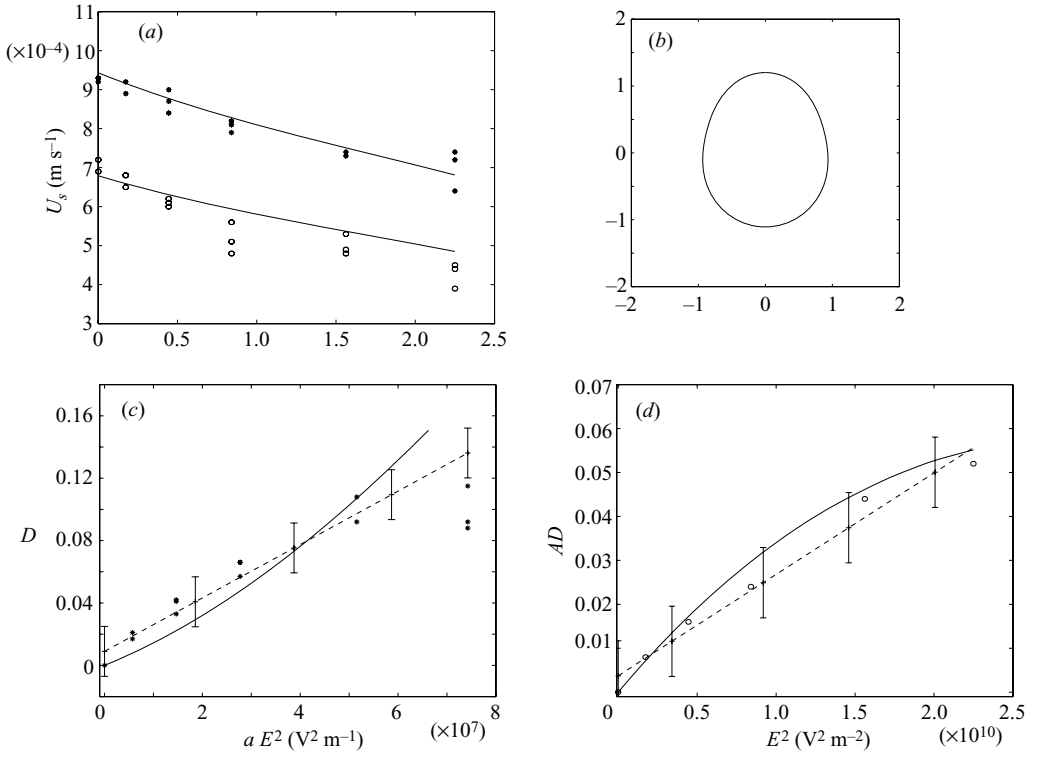

FIGURE 9. Theoretical fit of data, (*a*) settling velocity; (*b*) shape distortion at $E = 125\,\mathrm{KV\,m^{-1}}$; (*c*) deformation D and (*d*) asymmetric deformation AD with properties $\sigma = 2.4 \times 10^{-12}\,\mathrm{S\,m^{-1}}$, $\mu = 1.4\,\mathrm{kg\,ms^{-1}}$, $\gamma = 5 \times 10^{-3}\,\mathrm{N\,m^{-1}}$, $\varepsilon = 8$, $R = 1.55$, $Q = 0.35$, $M = 0.357$.

terms always increase the prolate deformation. Notice that we only calculate the correction to the deformation due to charge convection; there are also higher-order terms in shape distortion (Ajayi 1978) and some cross-terms from both of them. So this discrepancy might also arise from these higher-order terms.

Quantitative comparison between the theory and experiment is made difficult because of the lack of accurate properties for the fluids. When we evaluate the theory for the accepted values of parameters in table 1, the theoretical results do not make a close prediction: the deformation is predicted to be oblate and the settling velocity is predicted to increase with electric field, which are obviously contrary to the experimental results.

The quantitative comparison is very sensitive to the dielectric constant and conductivity of the fluids. Knowing that castor oil easily absorbs water, we assume the dielectric constant of castor oil can be higher than the reported value. Also PMM is one kind of thermal silicone fluid, and its conductivity is sensitive to temperature, i.e. the conductivity at 25 °C (table 1) is 100 times less than that at 50 °C. Finally, there is no agreed value for the conductivity of castor oil. A reasonable choice of parameters in which we vary both the dielectric constant and conductivity of the fluids, $\sigma = 2.4 \times 10^{-12}\,\mathrm{S\,m^{-1}}$, $\mu = 1.4\,\mathrm{kg\,ms^{-1}}$, $\gamma = 5 \times 10^{-3}\,\mathrm{N\,m^{-1}}$, $\varepsilon = 8$, $\mathrm{R} = 1.55$, $\mathrm{Q} = 0.35$, $\mathrm{M} = 0.357$, gives the fit to the data shown in figure 9. All the symbols in figure 9 have the same meaning as before, and the solid lines are the theoretical fits. This choice of parameters can fit the deformation and settling velocity very well. When we include

the higher-order terms in the power series expansion of settling velocity (equations (29*b*) and (34*b*)), the theory can even fit the experimental measurements at higher fields. As can be seen from figure 9(*b*), the shape distortion is asymmetric.

Besides this choice of properties, other combinations of physical parameters can also fit the data. We note that comparison between the theory and experiment is very sensitive to both dielectric constant and conductivity. A true comparison would require independent accurate measurements of the electrical properties, something we did not undertake for this study. However, from the qualitative comparison, we can draw the conclusions that:

(i) there is an effect of charge convection on the settling speed, as predicted by Spertell & Saville (1976);

(ii) the effect of shape distortion on settling speed is more important for larger drops than for small drops;

(iii) charge convection with settling drops leads to asymmetric distortion.

5. Conclusion

The deformation and settling velocity of a translating leaky dielectric liquid drop in a uniform electric field are investigated theoretically and experimentally at low Reynolds number. Perturbation methods are employed for small shape distortion (small Ca_E) and small charge convection (small Re_E), respectively, and the settling velocity is calculated by combining the corrections from the two contributions linearly at the lowest order. The dimensional result for the settling velocity reads, $U_s = U_H(1 + X_1 a E^2 + X_2 E^2)$, where U_H is the Hadamard–Rybczynski velocity, X_1 and X_2 are dimensional coefficients describing the effects of shape distortion and charge convection, respectively. For most fluid pairs in the experimental work of Torza *et al.* (1971) and Vizika & Saville (1992), the coefficients X_1 and X_2 have opposite sign, which indicates the existence of critical drop size determining whether the settling velocity is greater or less than U_H. The shape distortion due to charge convection has been calculated to second order. The expression of the linearized deformation shows that charge convection will enhance prolate deformation and decrease oblate deformation, which is consistent with the numerical results of Feng (1999). We also find X_1 is of the same sign as the Taylor deformation. So when Taylor's deformation is dominant and determines the sign of deformation, we have for prolate deformation $X_1 > 0$, and $X_1 < 0$ for oblate deformation.

Experimental measurements of the deformation and settling velocity of PMM drops in castor oil medium show qualitative agreement with the theory: the deformation D and the asymmetric deformation AD are proportional to E^2, and the change in the settling speed is quadratic in E, and shows the correct trends with drop size. We show it is possible to fit the data with reasonable choices for the physical parameters.

This work was supported by DOE, Office of Basic Energy Sciences, and by the NASA Microgravity Fluid Mechanics Program. We thank Professor Dudley Saville for encouraging us to do these experiments and for helpful comments.

REFERENCES

Adornato, P. M. & Brown, R. A. 1983 Shape and stability of electrostatically levitated drops. *Proc. R. Soc. Lond.* A **389**, 101–117.

Ajayi, O. O. 1978 A note on Taylor's electrohydrodynamic theory. *Proc. R. Soc. Lond.* A **364**, 499–507.

Chang, L. S., Carleson, T. E. & Berg, J. C. 1981 Heat and mass transfer to a translating drop in an electric field. *Intl J. Heat Mass Transf.* **25**, 1023–1030.

Feng, J. Q. 1999 Electrohydrodynamic behaviour of a drop subjected to a steady uniform electric field at finite electric Reynolds number. *Proc. R. Soc. Lond.* A **455**, 2245–2269.

Keh, H. J. & Chen, P. Y. 2001 Slow motion of a droplet between two parallel plane walls. *Chem. Engng Sci.* **56**, 6863–6871.

Landau, L. D. & Lifshitz, E. M. 1959 *Fluid Mechanics*. Pergamon.

Leal, L. G. 1992 *Laminar Flow and Convective Transport Processes: Scaling Principles and Asymptotic Analysis*. Butterworth–Heinemann.

Melcher, J. R. & Taylor, G. I. 1969 Electrohydrodynamics: a review of the role of interfacial shear stresses. *Annu. Rev. Fluid Mech.* **1**, 111–146.

Saville, D. A. 1997 Electrohydrodynamics: the Taylor–Melcher leaky dielectric model. *Annu. Rev. Fluid Mech.* **29**, 27–64.

Spertell, R. B. 1974 On the roles of convective and diffusive processes in the electrohydrodynamics of small particles and suspensions. PhD thesis, Princeton University.

Spertell, R. B. & Saville, D. A. 1976 The role of electrohydrodynamic phenomena in the motion of drops and bubbles. In *Proc. Intl Colloq. Drops Bubbles* (ed. M. Plesset), vol. 1, pp. 106–121. California Institute of Technology, Pasadena.

Taylor, G. I. 1966 Studies in electrohydrodynamics. I. The circulation produced in a drop by an electric field. *Proc. R. Soc. Lond.* A **291**, 159–166.

Taylor, T. D. & Acrivos, A. 1964 On the deformation and drag of a falling viscous drop at low Reynolds number. *J. Fluid Mech.* **18**, 466–476.

Torza, S., Cox, R. G. & Mason, S. G. 1971 Electrohydrodynamic deformation and burst of liquid drops. *Phil. Trans. R. Soc.* A **269**, 295–319.

Vizika, O. & Saville, D. A. 1992 The electrohydrodynamic deformation of drops suspended in liquids in steady and oscillatory fields. *J. Fluid Mech.* **239**, 1–21.

Wacholder, E. & Weihs, D. 1972 Slow motion of a fluid sphere in the vicinity of another sphere or a plane boundary. *Chem. Engng Sci.* **27**, 1817–1828.

Ward, T. & Homsy, G. M. 2001 Electrohydrodynamically driven chaotic mixing in a translating drop. *Phys. Fluids* **13**, 3521–3525.

Ward, T. & Homsy, G. M. 2003 Electrohydrodynamically driven chaotic mixing in a translating drop II. Experiments. *Phys. Fluids* **15**, 2987–2994.